MEMS Reconfigurable Broadband Patch Antenna for Conformal Applications

Michael D. Wright, *Student Member, IEEE*, William Baron, Jason Miller, James Tuss, David Zeppettella, and Mohammod Ali, *Senior Member, IEEE*

***Abstract*— An MEMS reconfigurable broadband pixelated patch antenna is introduced for conformal applications, such as in aircrafts or vehicles. The proposed design considers structural fiberglass composite, Rohacell foam, structural epoxy, ultrathin graphite fibers, and conductive epoxy to be the materials of choice. A nonconventional method of MEMS switch installation is developed and used, which requires connecting the MEMS chips to the antenna or feed traces using very small amounts of conductive epoxy and then curing the specimen in an oven. The proposed fabrication and assembly process is a low temperature process and is not limited in terms of specimen size. The proposed reconfigurable antenna has three reconfiguration states that allow it to operate from 1.13 to 1.7 GHz with 3–7 dBi gain, excellent radiation patterns, and low cross polarization.**

***Index Terms*— Broadband, conformal, MEMS, patch, reconfigurable, structural.**

I. Introduction

ANTENNA frequency, pattern, and polarization reconfiguration have been attempted using discrete p-i-n diode, photodiode, RF MEMS, and GaAs switches [1]–[37]. Among the classes of reconfigurable antennas, the pixelated reconfigurable antenna [11], [23], [28]–[35] has drawn interests among researchers and engineers because of the massive scope or opportunity for reconfiguration.

The DARPA Reconfigurable Aperture Program allowed reconfiguring elements of metal patches to form broadside and endfire patterns [11] with the help of discrete GaAs semiconductor switches. In [28], a pixelated monopole antenna reconfigured using RF MEMS switches was introduced. In [29], discrete MEMS reconfigurable pixelated patch antennas were designed for beam direction change. In [23], a pixelated patch antenna, including monolithically integrated MEMS, was proposed for multifrequency reconfiguration within 3–5 GHz.

Unlike previous works on pixelated reconfigurable antennas, this paper focuses on the design and development of an RF MEMS reconfigurable, conformal patch antenna, which can be integrated into a mechanical structure and become a part of the structure, such as an aircraft wing or fuselage. Unlike traditional bolt on antennas, the proposed antenna is designed under structural geometrical constraints. Furthermore, likely for the first time, the integration of a multitude of RF MEMS switches into a structural environment to reconfigure such an antenna is proposed. Our previous works in this topic area can be found in [32]–[35].

The work presented in this paper builds on and goes far beyond our prior works. The specific advances presented as compared to our own conference papers are the experimental design and development of an MEMS reconfigurable pixelated structurally embeddable broadband patch antenna that includes the following:

1) a new nontraditional method of flip-chip assembly of RF MEMS switches using minute amounts of conductive epoxy that are subsequently cured in an oven;
2) the investigation and evaluation of the electromagnetic interference (EMI) between the dc bias traces/wires and the antenna;
3) the mitigation of such EMI using another new nontraditional technique of embedding ultrathin (diameter less than 0.1 mm) graphite dc bias traces into the antenna and feed substrate specimens.

These approaches together demonstrate that an MEMS reconfigurable structurally embeddable antenna can be built for wide contiguous frequency reconfiguration (1.13–1.7 GHz) and good gain (3–7 dBi). The antenna has an effective volume of $0.3\,\lambda \times 0.26\,\lambda \times 0.08\,\lambda$, where λ is the free-space wavelength corresponding to the lowest frequency of operation.

This paper is organized as follows. First, the antenna geometry and reconfiguration states are described followed by the rationale for the choice of materials and device to develop a structurally embeddable antenna. Second, reconfigurable antenna fabrication and integration techniques are presented and their associated outcomes and challenges are discussed. Experimental results of a structural MEMS reconfigurable antenna are presented. Third, the performance degradation of the reconfigurable antenna caused by dc bias traces and wires

Manuscript received April 2, 2017; revised March 4, 2018; accepted March 7, 2018. Date of publication March 26, 2018; date of current version May 31, 2018. This work was supported by the Air Force Research Laboratory, Wright Patterson Air Force Base, under Contract 15-S2606-04-C18. Cleared for Public Release—Case Number: 88ABW-2018-1034. *(Corresponding author: Mohammod Ali.)*

M. D. Wright and M. Ali are with the Department of Electrical Engineering, University of South Carolina, Columbia, SC 29208 USA (e-mail: wrigh297@email.sc.edu; alimo@cec.sc.edu).

W. Baron, J. Miller, and D. Zeppettella are with the Air Force Research Laboratory, Wright Patterson Air Force Base, OH 45433 USA (e-mail: william.baron.1@us.af.mil; jason.miller.67.ctr@us.af.mil; david.zeppettella@us.af.mil).

J. Tuss, retired, was with the Air Force Research Laboratory, Wright Patterson Air Force Base, OH 45433 USA (e-mail: maggietuss@aol.com).

Color versions of one or more of the figures in this paper are available online at http://ieeexplore.ieee.org.

Digital Object Identifier 10.1109/TAP.2018.2819818

is investigated. Finally, the results of an experimental prototype of a reconfigurable antenna containing RF MEMS switches and graphite dc bias traces are presented that demonstrate performance over the frequency band outlined above.

II. Antenna Configuration, Materials, and Device Integration

A. Antenna Configuration

Fig. 1 shows the general geometry of the reconfigurable structural antenna. It contains three substrates. Substrate 1 (1.6 mm thick fiberglass epoxy) contains a slot and a 50 Ω microstrip feedline. The feedline contains two MEMS switches that control two matching stubs [see Fig. 1(c)] that will be described later. The middle substrate, i.e., substrate 2 is a 17 mm thick Rohacell foam core ($\varepsilon_r = 1.06$ and $\tan\delta = 0.0003$). Substrate 3 (0.4 mm thick fiberglass epoxy) contains conducting pixels that can be joined or disconnected to achieve the various antenna frequency reconfiguration states. The top, middle, and bottom substrates are bonded together using thin (1–2 mil) layers of structural epoxy. A fourth dielectric material which will be a superstrate (also fiberglass) would eventually be needed to be placed on a finished antenna, e.g., on top of substrate 3 [34]. It is called the outer mold line for a structurally embeddable antenna.

Substrate 1 contains 11 × 9 conducting copper pixels each 5 mm × 5 mm. Each pixel is separated from its neighbor by a 2.5 mm distance. The slot on the ground plane of substrate 1 is 45 mm long and 4.5 mm wide for the frequency of interest. The inner 9×7 pixels (shown in green color) are all connected to each other by 1 mm wide copper bridges. There are four rows of pixels that are shown in black color that can be reconfigured using four rows of MEMS switches [see Fig. 1(b)]. With no switches ON, the inner 9 × 7 pixels create the Highband configuration of the pixel patch. With Rows 1 and 2 of switches ON, the antenna achieves its Midband configuration. Finally, with all four rows of switches ON, the antenna achieves its Lowband configuration. For the Highband configuration, the two switches on the feedline remain OFF [see Fig. 1(c)]. For the Midband configuration, the first switch that is near the feedline is turned ON. And finally for the Lowband configuration, both switches on the feedline are turned ON. In total, substrate 1 contains 2 MEMS and substrate 3 contains 36 MEMS.

The substrate materials, their thicknesses, the pixels, their sizes, the slot size, and the stub dimensions were optimized using HFSS simulations considering ideal switches in our prior work [33], [34]. A summary of all materials and dimensions is listed in Table I.

B. Materials, Devices, and Their Assembly or Integration

Fiberglass composites have been reported to develop structural antennas that form sandwich structures [38]. A dielectric substrate that has similar RF properties compared with fiberglass composites is FR4 ($\varepsilon_r = 4.4$ and $\tan\delta = 0.02$). Since FR4 is readily available, it was selected to fabricate the proposed antenna. RF MEMS (RMSW101) switches were considered for the proposed reconfigurable antenna because

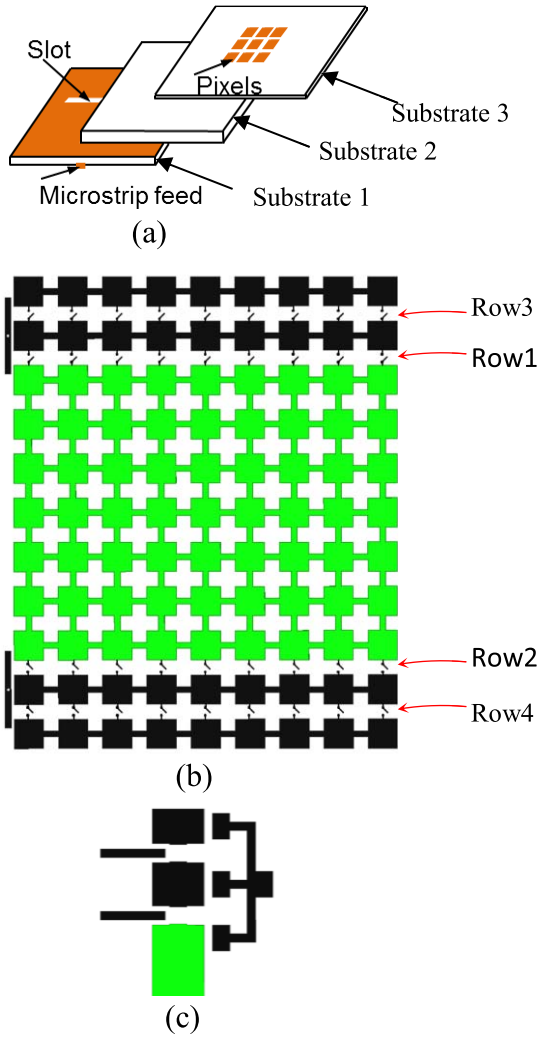

Fig. 1. General geometry of the MEMS reconfigurable structural antenna. Reconfigured pixels are shown in black color. (a) Stack-up. (b) Pixels. (c) Stubs.

TABLE I
Materials and Their Properties

Item	Type	Thickness	Properties
Substrate 1	FR4	1.6 mm	$\varepsilon_r = 4.4$, $\tan\delta = 0.02$
Substrate 2	Rohacell	17 mm	ε_r=1.06, $\tan\delta$=0.0003
Substrate 3	FR4	0.4 mm	$\varepsilon_r = 4.4$, $\tan\delta = 0.02$
Switch	RMSW101	N/A	0.2 dB insertion loss, 40 dB isolation
Conductive Epoxy	EPO-TEK H20E	N/A	N/A

of their low insertion loss (0.2 dB) and high isolation (greater than 20 dB) [40].

The RMSW101 switch was installed and integrated to the antenna and feedline traces using the flip chip method using conductive epoxy (EPO-TEK H20E). The substrate containing all switches was then placed in an oven and cured at 120 °C for 1 h. The details on the materials, devices, and switch integration can be found in [39].

DC bias voltage is supplied to the RF MEMS through four dc busbars, which are located on the bottom of the patch

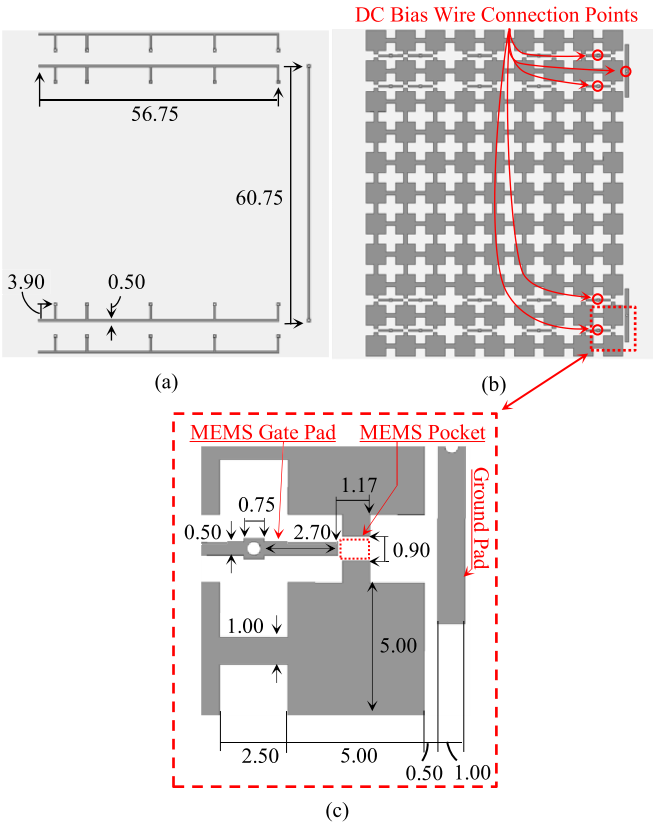

Fig. 2. Pixel patch substrate trace dimensions. (a) Underside of substrate with dc busbars. (b) Upper surface of substrate with pixel patch traces. (c) Area of pixel patch showing traces in the vicinity of the MEMS pocket.

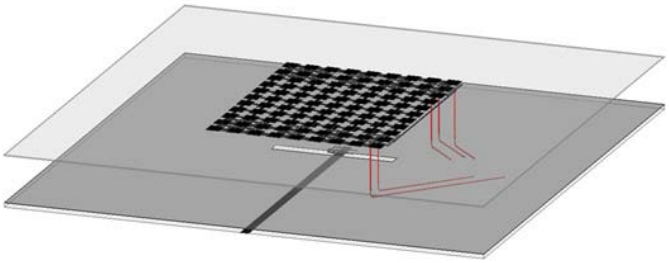

Fig. 3. Illustrating the five dc bias wires in red color. The foam substrate is hidden to show the wires.

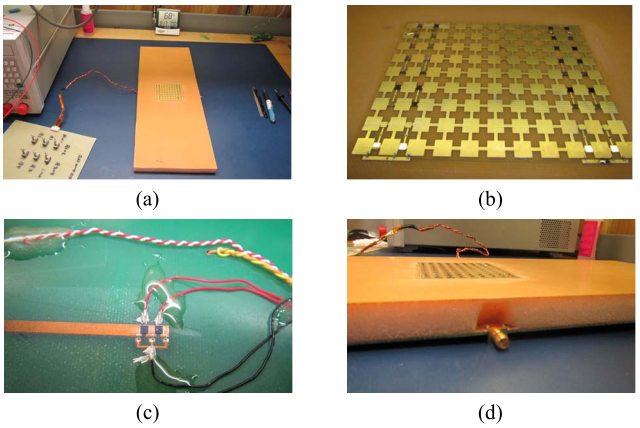

Fig. 4. Photographs of Antenna Prototype 1. (a) Structural antenna connected to switch control board. (b) Pixelated patch with MEMS. (c) Feedline with dc bias wires and MEMS. (d) Side view of structural antenna.

substrate or substrate 3. This is shown in Fig. 2. Each busbar biases all switches in that row, where the busbar is connected to the individual gate pads of the MEMS through conducting vias. Utilizing the busbars this way allows all 36 RF MEMS to be controlled through a total of five dc bias wires (see Fig. 3), one wire for each row of RF MEMS, and one ground wire which is connected to both ground pads through the dc ground busbar. There are five 40 kΩ dc bias resistors for the four rows of switches on substrate 1. Similarly, there are 3 40 kΩ dc bias resistors for the MEMS on the feed substrate.

III. Results

A. Experimental Antenna Prototype 1 and Measured Results

To ensure that the electrical connection of RF MEMS using conductive epoxy is acceptable, several 50 Ω microstrip transmission line specimens were fabricated on 1.6 mm thick FR4 substrates, where MEMS switches could be installed using the above technique. A dummy transmission line containing no switch was also fabricated and measured. The maximum, per switch, insertion loss measured was between 0.075 and 0.2 dB, which is no worse than the insertion loss measured using wire bonding methods for MEMS [40]. The measured return loss was better than 20 dB, while the isolation was more than 40 dB.

Based on the methods and procedures described above, a prototype reconfigurable antenna was fabricated and tested. We will refer to this antenna as Antenna Prototype 1.

Photographs of Antenna Prototype 1 (470 mm × 178 mm × 19 mm) can be seen from Fig. 4. To control the MEMS switches, an external circuit board with toggle switches was also fabricated [see Fig. 4(a)].

Measured S11 versus frequency data of Antenna Prototype 1 is shown in Fig. 5. It is clear that the antenna has excellent S11 performance and bandwidth in the Highband (−10 dB bandwidth of 1.3–1.7 GHz or 26.7%). When the switches in Rows 1 and 2 (see Fig. 1) are turned ON by applying 90 V to the MEMS in those rows, the antenna reconfigures to the Midband shown using the red trace in Fig. 5. Antenna state reconfiguration from Highband to Midband is clear, but the S11 results are poor. The S11 is less than −10 dB only within a very narrow frequency range. Similar situation arises when all of the rows of switches are turned ON. The antenna does reconfigure to the Lowband as seen from the blue trace but again has poor S11 performance. Clearly, the Midband and the Lowbands have problems with impedance matching to the 50 Ω feedline.

Measured gain and radiation patterns of this antenna are shown in Figs. 6 and 7, respectively. Gain and patterns were measured for a fee inside a Satimo anechoic chamber. Since there were three reconfiguration states that constituted three separate measurements, we selected fewer data points to conserve measurement costs. Gain versus frequency data was curve fitted in MATLAB to generate the plots shown in Fig. 6 where the actual measured gain data appear as discrete points on the curves. As seen, the gain results follow

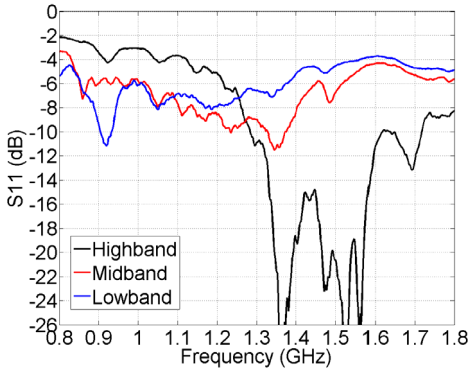

Fig. 5. Measured S11 as a function of frequency for Antenna Prototype 1.

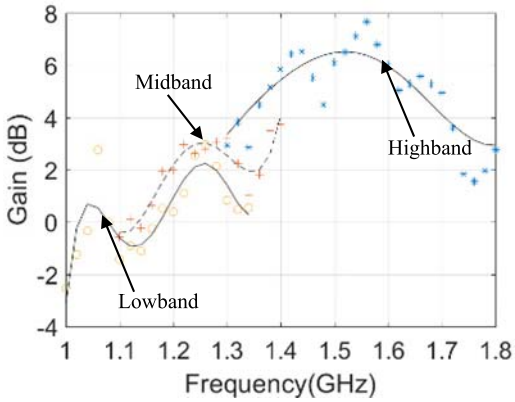

Fig. 6. Measured gain of Antenna Prototype 1.

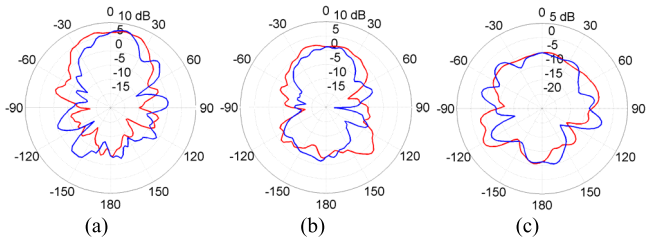

Fig. 7. Measured radiation patterns for Antenna Prototype 1. (a) Highband at 1.56 GHz. (b) Midband at 1.30 GHz. (c) Lowband at 1.06 GHz. Red: E-plane. Blue: H-plane.

the S11 results shown in Fig. 5. The antenna in the Highband has a gain between 3 and 7.5 dB within 1.3–1.7 GHz. Since the antenna S11 results are poor in both the Midband and Lowband, the gain plots do not exhibit clear signs of separate reconfigured bands.

The radiation patterns in Fig. 7(a) reveal that although the Highband exhibits greater than 5 dB gain, the E- and H-plane patterns show signs of deformation and asymmetry. The Midband gain is low and the patterns show asymmetry and deformation [see Fig. 7(b)]. The Lowband patterns do not appear to look like the pattern of a directional patch antenna.

It is clear from the measured results of Antenna Prototype 1 that the reconfigurable antenna had low gain, poor S11, and deformed patterns especially in the reconfigured Midband and Lowband. During the measurements of S11, it was determined that the antenna performance degradations observed were

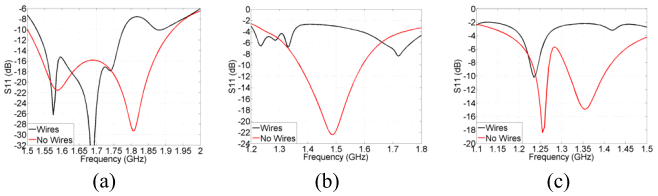

Fig. 8. Simulated S11 data showing the effect of including the dc bias wires to the antenna. (a) Highband. (b) Midband. (c) Lowband.

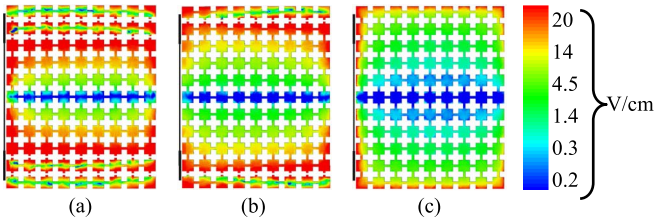

Fig. 9. Simulated electric field distributions for the pixel patch and dc bus bar traces without the introduction of dc bias wiring. (a) Highband at 1.70 GHz. (b) Midband at 1.49 GHz. (c) Lowband at 1.35 GHz.

caused by the EMI caused to the antenna by the dc bias traces and wiring. Any movement of the bias wires that were connected to the wires shown in Fig. 3 would change the S11. Our previous HFSS simulation studies [33], [34] up to the fabrication of Antenna Prototype 1 did not fully consider the effects of the presence of the dc bias traces and wires.

B. Identifying the Cause of Performance Degradation

The EMI caused by the dc bias wiring in the presence of the dc busbars was studied from an EM field point of view using HFSS. Ideal switches were considered for the model (short for ON and open for OFF). Shorts were created using copper strips. The dc bias wires were modeled using 0.25 mm diameter copper wires.

Simulated S11 plots of the Highband, Midband, and Lowband before and after including the dc bias wires are shown in Fig. 8. The Highband, although affected by the wires, still shows S11 bandwidth within −10 dB S11. The wires significantly deteriorate the Midband and Lowband, as can be seen from Fig. 8(b) and (c).

Field simulation results elucidate the deleterious effects of the dc bias wires further. Fig. 9 shows the simulated electric field distributions for the three reconfiguration states before the inclusion of the dc bias wires. Although the electric field distributions in Fig. 9 do not precisely conform to the standard electric field distribution of a microstrip patch antenna due to the pixelated antenna geometry and dc busbars on the underside of the substrate, they do show the outlines of three antennas, small, medium, and long in size. The maximum field intensity occurs mostly along the edges of the last rows of pixels intended for that reconfiguration state, and the minimum intensity occurs at the center of the pixel patch for all reconfiguration states.

Fig. 10 shows the electric field magnitude distributions after the inclusion of the dc bias wires. As seen, the Highband E-fields are deformed, but still retain some semblance to the original E-field magnitude distribution. The field distributions

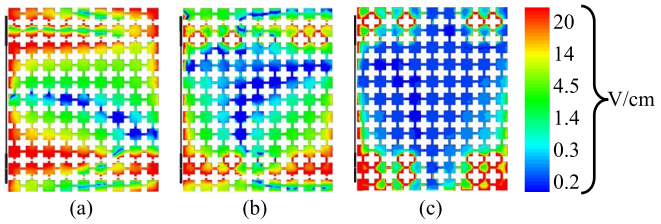

Fig. 10. Simulated electric field distributions for the pixel patch after the introduction of the dc bias wiring. (a) Highband at 1.7 GHz. (b) Midband at 1.49 GHz. (c) Lowband at 1.35 GHz.

for the Midband and Lowband are completely deformed and are no longer recognizable as the electric fields of a typical patch antenna. These detrimental effects persisted for any reasonable length of bias wires. These subsequent findings from HFSS simulations were presented in a conference paper [35]. Attempt to reduce the EMI using 40 kΩ chip resistors between the dc busbars and the wires was unsuccessful.

C. Performance Improvement Using Graphite DC Bias Traces—Simulation Results

In the literature, there are reports of RF MEMS switches being biased using dc traces made from high sheet-resistance alloys, such as Ni-Chrome [23]. Typically, these are extremely thin traces that are fabricated in a microelectronic cleanroom environment using high-temperature processes on small semiconductor substrates, e.g., high-resistivity Si. Such a method is not feasible for a structural reconfigurable antenna fabrication because composite panels require low-temperature fabrication (less than 150 °C) in order to prevent delamination. For a structural antenna, a compromise choice will be to use manually installed graphite fibers (conductivity of approximately 70 000 S/m) to provide the dc bias to the MEMS. Graphite is not an ideal choice from an RF point of view because it does not provide very high sheet-resistance. However, due to its widespread usage in composite structures and the fact that it can be installed manually led us to investigate its feasibility to fabricate the dc busbars using it.

Considering 0.1 mm diameter graphite fibers, the resistance is 46.2 Ω/in. We hypothesized that long bias lines with optimized geometry should provide high enough resistance to allow dc biasing of the MEMS while keeping the RF isolated from it. Multiple geometries and arrangements of dc bias traces using graphite were considered to optimize antenna gain and S11 performance. Attention was also paid to geometries that can be manually fabricated. Although the dc biasing using straight graphite fibers is preferred a bias layout consisting of both straight and zigzag geometries (see Fig. 11) turned out to be optimum. Notwithstanding that many other bias geometries can also be found to allow similar or perhaps a better performance. The layout shown in Fig. 11(b) comprises of a series of 10.5 mm sections of graphite fibers alternating at 45° and −45° angles to the E-plane of the antenna. The length of the fourth cycle of ±45° was shortened to 5.2 mm to account for the closer spacing of the two vias at that position.

Using the graphite busbar schemes shown and described above, simulations were conducted for the low, mid, and high bands. A Rohacell foam core was added to the new models.

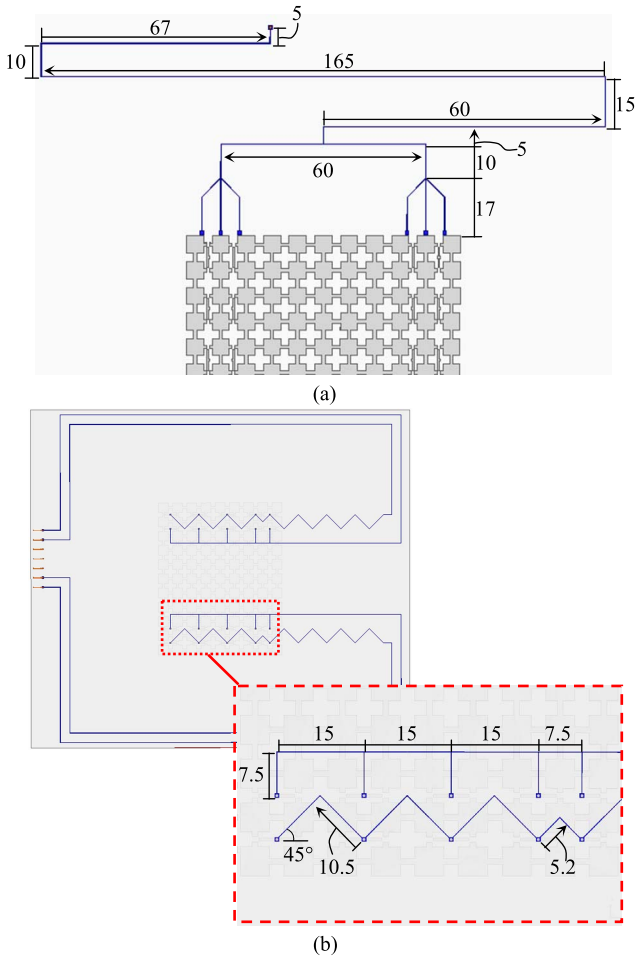

Fig. 11. Layout of the sawtooth-shaped graphite dc bias lines (all dimensions in millimeters). (a) Simplified pixel patch ground connection graphite line on the top side of the patch substrate. (b) New sawtooth arrangement for the graphite lines on the underside of the patch substrate.

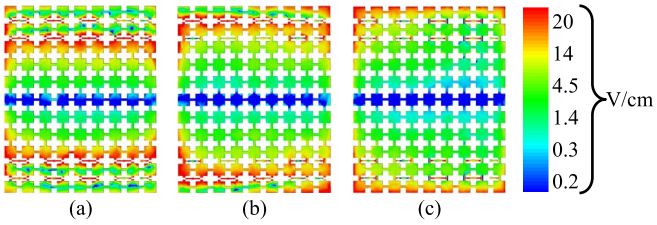

Fig. 12. Electric field magnitudes for the pixelated patch with high-impedance sawtooth-shaped graphite dc bias lines. (a) Highband at 1.6 GHz. (b) Midband at 1.4 GHz. (c) Lowband at 1.2 GHz.

The foam core was bounded on the upper and lower surfaces by 2 mil thick dielectric layers to approximate structural epoxy. The RF MEMS switches were approximated as shorts and opens to represent the ON and OFF states, respectively.

The simulated electric field magnitudes of Fig. 12 clearly show that the fields for all bands now in general conform to what is expected from the pixelated patch antenna. This confirms that the EMI effects due to copper dc bias traces and wires can be mitigated using traces made using thin graphite fibers.

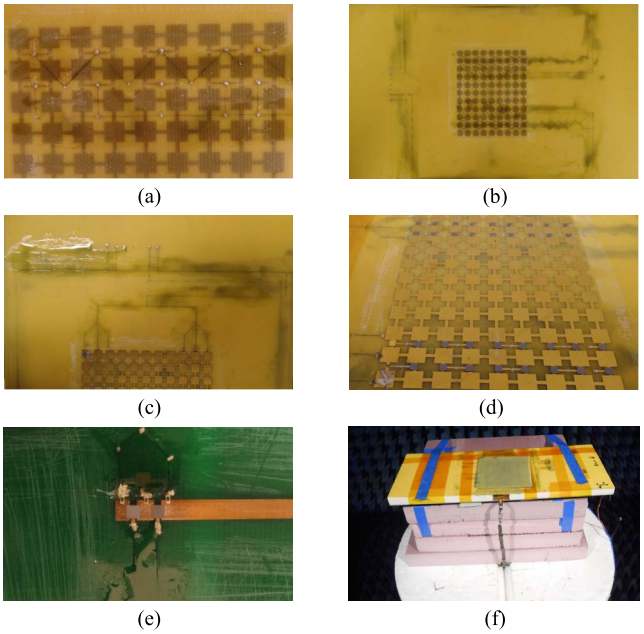

Fig. 13. Photographs of Prototype 2 with high-impedance sawtooth-shaped graphite dc bias lines. (a) Section of graphite lines on underside of patch substrate before protective coat of epoxy. (b) Underside of patch substrate with graphite lines coated in epoxy. (c) Patch ground connection with protective coat of epoxy. (d) Pixel patch with 36 MEMS installed. (e) Feedline with both MEMS installed. (f) Completed antenna on testing pedestal at WRCNC [41].

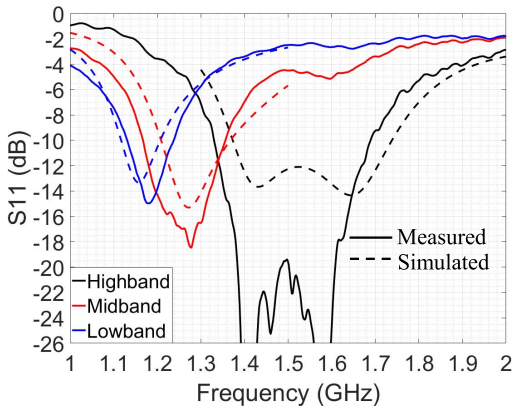

Fig. 14. Simulated and measured S11 for all three reconfiguration states for the aperture coupled MEMS reconfigurable pixelated patch antenna with high-impedance sawtooth-shaped graphite dc bias lines.

D. Experimental Prototype Antenna 2 and Measured Results

An experimental prototype Antenna 2 with all the graphite dc busbars, MEMS switches, and copper wires was fabricated (see Fig. 13) and tested. Structural epoxy was used to glue the patch substrate to the foam core in the vicinity of the pixel patch.

On top of the antenna, a 2 mm thick Rohacell foam followed by a 1.3 mm thick fiberglass dielectric superstrate were added as suggested by our previous work [34].

Measured S11 results for Antenna 2 are shown in Fig. 14. For comparison, simulations were also performed representing this completed specimen using HFSS. The "ON" and "OFF" states of each MEMS switch were modeled using a 2 Ω resistor and a 20 fF capacitor, respectively, to reflect the measured insertion loss and isolation of each switch described in Section III-A.

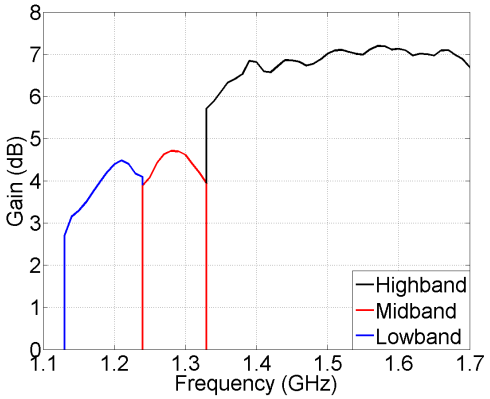

Fig. 15. Measured gain versus frequency for the reconfiguration states.

Equation (1) [42] for insertion loss or isolation was used to obtain the equivalent resistance or capacitance to represent the MEMS

$$\mathrm{IL} = -20\log_{10}\left|\frac{2Z_0}{2Z_0 + Z_d}\right| dB \tag{1}$$

where $Z_0 = 50\ \Omega$ and Z_d is the MEMS impedance in the ON or OFF state.

Part of the structural epoxy (in the form of a film) bled into the foam while being cured. To account for that the dielectric constant of the foam adjacent to the joints was increased in the simulation model. The simulation model contained the following dielectric layers in sequence from the top: 1) 1.3 mm thick FR4 superstrate; 2) 2 mm thick foam with $\varepsilon_r = 1.2$; 3) 0.05 mm thick structural epoxy with $\varepsilon_r = 4.2$; 4) 0.4 mm thick FR4 (containing the pixel patch, MEMS, and dc bias); 5) 2 mm thick foam with $\varepsilon_r = 2.1$; 6) 13 mm thick foam with $\varepsilon_r = 1.06$; 7) 2 mm thick foam with $\varepsilon_r = 2.1$; 8) 0.05 mm thick structural epoxy with $\varepsilon_r = 4.2$; and 9) 1.6 mm thick FR4 (containing the slot, the microstrip feedline, MEMS, and matching stubs).

From Fig. 14, it is clear that the simulated resonances are in good agreement with the measured S11 responses. From either sets of data, it can be seen that the antenna shows three clear reconfiguration states each under −10 dB S11. These data are a significant leap from what was observed before in Fig. 5.

Antenna radiation patterns and gain were measured inside a Satimo anechoic chamber [41]. The gain data of each reconfiguration state are plotted at frequencies where S11 ≤ -9.5 dB and are shown in Fig. 15. As seen, every reconfiguration state has gain above 3 dBi, and each reconfiguration state provides value to the antenna in terms of total frequency coverage. Clearly, the antenna has measured gain between 3 and 7 dBi from about 1.13 to 1.7 GHz, i.e., a frequency ratio of 1.5:1. As a matter of fact, gain continues beyond 1.7 GHz but was not measured because S11 exceeded −9.5 dB.

Simulated gain (not shown in Fig. 15) had peak values of 6.5, 5.5, and 4.7 dBi at 1.6, 1.28, and 1.16 GHz, respectively. Measured peak gain values are 7.2, 4.7, and 4.5 dBi at 1.6, 1.28, and 1.22 GHz, respectively. Simulated minimum gain was 3.4 dBi at 1.1 GHz, while measured minimum gain was 3 dBi at 1.14 GHz.

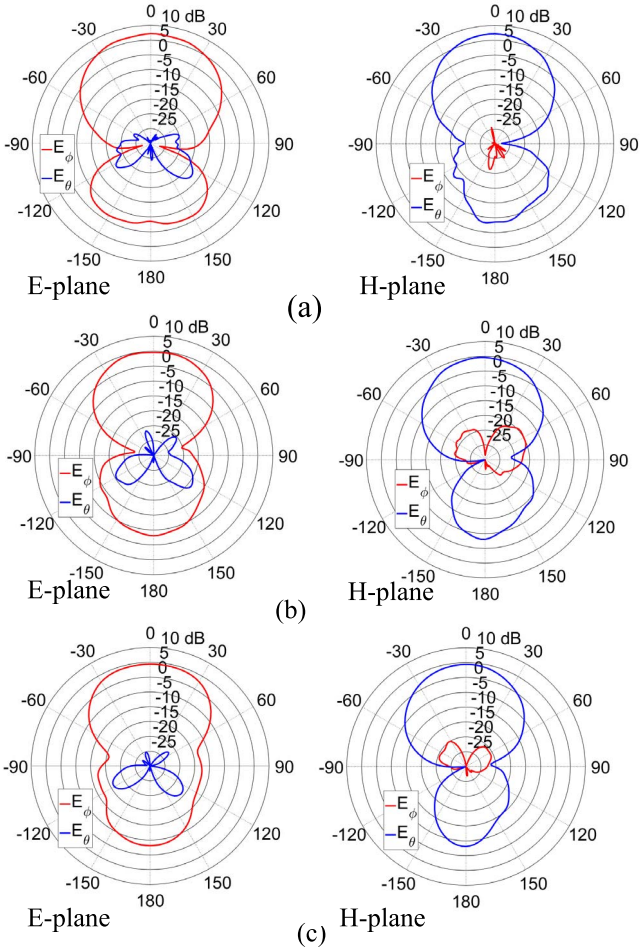

Fig. 16. Measured radiation patterns. (a) Highband at 1570 MHz. (b) Midband at 1280 MHz. (c) Lowband at 1220 MHz.

Clearly, more bandwidth can come from the high band by further optimizing the substrate thicknesses (especially the foam thicknesses), slot, and stubs. An additional high-band state can be created by adding two more rows of switches making a new 5×9 pixel state. Measured radiation patterns are shown in Fig. 16. Plots show that every reconfiguration state maintains a radiation pattern expected from an aperture coupled patch antenna over the entire span of its respective frequency range.

IV. Discussion

Comparing the simulation and measurement results in Fig. 14, it can be seen that there are small frequency shifts between the two. This can be attributed primarily to the effect of the structural epoxy that bled into the foam core. Also there perhaps was some variability in the dielectric constant of the substrate material that was actually used in the fabrication compared to what was used in the simulation model. Also there were assumptions made about the nature of the graphite busbars in the simulation model which may have been slightly different from what was actually fabricated.

Also from Fig. 15, it is apparent that the Lowband is not as well separated from the Midband. It should be clear from this paper that the bulk of our effort was placed on developing methods and techniques to realize an MEMS reconfigurable antenna that can be implemented into a structural environment. Fine-tuning antenna resonances was not a focus. Nevertheless, several approaches can be taken to make the low and midbands separated further to achieve even more bandwidth in the lower frequencies. These include redesigning the pixels, adding more pixels to the low band, redesigning the matching stubs, and increasing the thickness of the foam core.

V. Conclusion

This paper presents the experimental demonstration of an MEMS reconfigurable pixelated patch antenna for conformal applications such as that can be integrated into an aircraft or vehicle. The antenna design considers structural fiberglass composite, Rohacell foam, structural epoxy, ultrathin graphite fibers, and conductive epoxy to be the materials of choice. A nonconventional method of MEMS switch installation is introduced that entails connecting the MEMS chips to the antenna or feed traces using minute amounts of conductive epoxy and then curing the specimen in an oven. The whole fabrication and assembly process is a low-temperature process. Also the process is not limited in terms of specimen size.

The proposed reconfigurable antenna has three reconfiguration states that allow it to operate from 1.13 to 1.7 GHz. Within this bandwidth, the antenna has 3–7 dBi gain, good radiation patterns, and low cross polarization. The potentials to increase the bandwidth even further exist. This can be attempted by adding more reconfiguration states with the constraints that the slot length, foam height, stub dimensions, and so on are optimized.

References

[1] J. T. Bernhard, *Reconfigurable Antennas*. San Rafael, CA, USA: Morgan & Claypool, 2007.

[2] W. H. Wecdon and W. J. Payne, "MEMS-switched reconfigurable multiband antenna: Design and modeling," in *Proc. Antenna Appl. Symp.*, Monticello, IL, USA, Sep. 1999, pp. 203–231.

[3] J. T. Bernhard, R. Wang, R. Clark, and P. Mayes, "Stacked reconfigurable antenna elements for space-based radar applications," in *IEEE Antennas Propag. Symp. Dig.*, vol. 1. Jul. 2001, pp. 158–161.

[4] F. Yang and Y. Rahmat-Samii, "Patch antenna with switchable slot (PASS): Dual-frequency operation," *Microw. Opt. Technol. Lett.*, vol. 31, no. 3, pp. 165–168, Nov. 2001.

[5] D. Peroulis, K. Sarabandi, and L. P. B. Katehi, "A planar VHF reconfigurable slot antenna," in *IEEE Antennas Propag. Symp. Dig.*, vol. 1. Jul. 2001, pp. 154–157.

[6] F. Yang and Y. Rahmat-Samii, "A reconfigurable patch antenna using switchable slots for circular polarization diversity," *IEEE Microw. Wireless Compon. Lett.*, vol. 12, no. 3, pp. 96–98, Mar. 2002.

[7] J. Sor, C.-C. Chang, Y. Qian, and T. Itoh, "A reconfigurable leaky-wave/patch microstrip aperture for phased-array applications," *IEEE Trans. Microw. Theory Techn.*, vol. 50, no. 8, pp. 1877–1884, Aug. 2002.

[8] M. A. Ali and P. Wahid, "A reconfigurable Yagi array for wireless applications," in *IEEE Antennas Propag. Soc. Int. Symp. Dig.*, vol. 1. Jun. 2002, pp. 466–468.

[9] B. A. Cetiner, H. Jafarkhani, J.-Y. Qian, H. J. Yoo, A. Grau, and F. D. Flaviis, "Multifunctional reconfigurable MEMS integrated antennas for adaptive MIMO systems," *IEEE Commun. Mag.*, vol. 42, no. 12, pp. 62–70, Dec. 2004.

[10] V. K. Kunda, M. Ali, and H. S. Hwang, "Study and design of a multifunctional stacked microstrip patch antenna," in *Proc. IEEE Antennas Propag. Soc. Int. Symp. URSI/USNC Meeting*, vol. 3. Monterey, CA, USA, Jun. 2004, pp. 2603–2606.

[11] L. N. Pringle *et al.*, "A reconfigurable aperture antenna based on switched links between electrically small metallic patches," *IEEE Trans. Antennas Propag.*, vol. 52, no. 6, pp. 1434–1445, Jun. 2004.
[12] J. T. Bernhard, "Reconfigurable antennas," in *Encyclopedia of RF and Microwave Engineering*, K. Chang, Ed. New York, NY, USA: Wiley, 2005.
[13] G. Yang, M. Ali, and R. Dougal, "A multi-functional stacked patch antenna for wireless power beaming and data telemetry," in *IEEE Antennas Propag. Soc. Int. Sym. Dig.*, vol. 2A. Washington, DC, USA, Jul. 2005, pp. 359–362.
[14] S. Nikolaou *et al.*, "Pattern and frequency reconfigurable annular slot antenna using PIN diodes," *IEEE Trans. Antennas Propag.*, vol. 54, no. 2, pp. 439–448, Feb. 2006.
[15] G. H. Huff and J. T. Bernhard, "Integration of packaged RF MEMS switches with radiation pattern reconfigurable square spiral microstrip antennas," *IEEE Trans. Antennas Propag.*, vol. 54, no. 2, pp. 464–469, Feb. 2006.
[16] D. E. Anagnostou *et al.*, "Design, fabrication, and measurements of an RF-MEMS-based self-similar reconfigurable antenna," *IEEE Trans. Antennas Propag.*, vol. 54, no. 2, pp. 422–432, Feb. 2006.
[17] E. Erdil, K. Topalli, M. Unlu, O. A. Civi, and T. Akin, "Frequency tunable microstrip patch antenna using RF MEMS technology," *IEEE Trans. Antennas Propag.*, vol. 55, no. 4, pp. 1193–1196, Apr. 2007.
[18] J. T. Bernhard, "Reconfigurable antennas," in *Antenna Engineering Handbook*, J. Volakis, Ed., 4th ed. New York, NY, USA: McGraw-Hill, 2007.
[19] M. Ali, A. T. M. Sayem, and V. K. Kunda, "A reconfigurable stacked microstrip patch antenna for satellite and terrestrial links," *IEEE Trans. Veh. Technol.*, vol. 56, no. 2, pp. 426–435, Mar. 2007.
[20] S. Nikolaou, N. D. Kingsley, G. E. Ponchak, J. Papapolymerou, and M. M. Tentzeris, "UWB elliptical monopoles with a reconfigurable band notch using MEMS switches actuated without bias lines," *IEEE Trans. Antennas Propag.*, vol. 57, no. 8, pp. 2242–2251, Aug. 2009.
[21] A. Grau, J. Romeu, M.-J. Lee, S. Blanch, L. Jofre, and F. De Flaviis, "A dual-linearly-polarized MEMS-reconfigurable antenna for narrowband MIMO communication systems," *IEEE Trans. Antennas Propag.*, vol. 58, no. 1, pp. 4–17, Jan. 2010.
[22] B. A. Cetiner, G. R. Crusats, L. Jofre, and N. Biyikli, "RF MEMS integrated frequency reconfigurable annular slot antenna," *IEEE Trans. Antennas Propag.*, vol. 58, no. 3, pp. 626–632, Mar. 2010.
[23] A. G. Besoli and F. De Flaviis, "A multifunctional reconfigurable pixeled antenna using MEMS technology on printed circuit board," *IEEE Trans. Antennas Propag.*, vol. 59, no. 12, pp. 4413–4424, Dec. 2011.
[24] G. Yang, R. Islam, R. A. Dougal, and M. Ali, "A stacked patch antenna and switched feed network for wireless power beaming and data telemetry," *Prog. Electromagn. Res. C*, vol. 29, pp. 67–81, 2012.
[25] M. R. Islam, N. H. Chamok, and M. Ali, "Switched parasitic dipole antenna array for high-data-rate body-worn wireless applications," *IEEE Antennas Wireless Propag. Lett.*, vol. 11, pp. 693–696, 2012.
[26] M. R. Islam and M. Ali, "A 900 MHz beam steering parasitic antenna array for wearable wireless applications," *IEEE Trans. Antennas Propag.*, vol. 61, no. 9, pp. 4520–4527, Sep. 2013.
[27] D. E. Anagnostou, M. T. Chryssomallis, B. D. Braaten, J. L. Ebel, and N. Sepúlveda, "Reconfigurable UWB antenna with RF-MEMs for on-demand WLAN rejection," *IEEE Trans. Antennas Propag.*, vol. 62, no. 6, pp. 602–609, Feb. 2014.
[28] D. Rodrigo, Y. Damgaci, N. Biyikli, B. A. Cetiner, J. Romeu, and L. Jofre, "MEMS-reconfigurable antenna based on a multi-size pixelled geometry," in *Proc. 4th Eur. Conf. Antennas Propag. (EuCAP)*, Barcelona, Spain, Apr. 2010, pp. 1–4.
[29] D. Rodrigo and L. Jofre, "Frequency and radiation pattern reconfigurability of a multi-size pixel antenna," *IEEE Trans. Antennas Propag.*, vol. 60, no. 5, pp. 2219–2225, May 2012.
[30] D. Rodrigo, B. A. Cetiner, and L. Jofre, "Frequency, radiation pattern and polarization reconfigurable antenna using a parasitic pixel layer," *IEEE Trans. Antennas Propag.*, vol. 62, no. 6, pp. 3422–3427, Jun. 2014.
[31] S. Song and R. D. Murch, "An efficient approach for optimizing frequency reconfigurable pixel antennas using genetic algorithms," *IEEE Trans. Antennas Propag.*, vol. 62, no. 2, pp. 609–620, Feb. 2014.
[32] M. Ali, N. Bishop, W. Baron, B. Smyers, J. Tuss, and D. Zeppettella, "A MEMS reconfigurable pixel microstrip patch antenna for conformal load bearing antenna structures (CLAS) concept," in *Proc. IEEE Antennas Propag. Soc. Int. Symp.*, Memphis, TN, USA, Jul. 2014, pp. 1093–1094.
[33] N. Bishop, W. Baron, J. Miller, J. Tuss, D. Zeppettella, and M. Ali, "Aperture coupled MEMS reconfigurable pixel patch antenna for conformal load bearing antenna structures (CLAS)," in *Proc. IEEE Antennas Propag. Soc. Int. Symp.*, Memphis, TN, USA, Jul. 2014, pp. 1091–1092.
[34] M. Wright, W. Baron, J. Miller, J. Tuss, D. Zeppettella, and M. Ali, "Superstrate configurations for a MEMS reconfigurable pixelated patch antenna for CLAS," in *Proc. IEEE Int. Symp. Antennas Propag. Soc.*, Vancouver, BC, Canada, Jul. 2015, pp. 2387–2388.
[35] M. Wright, W. Baron, J. Miller, J. Tuss, D. Zeppettella, and M. Ali, "Effect of bias traces and wires on a MEMS reconfigurable pixelated patch antenna," in *Proc. IEEE Antennas Propag. Soc. Int. Symp.*, Fajardo, Puerto Rico, Jun. 2016, pp. 1429–1430.
[36] N. H. Chamok, M. H. Yılmaz, A. Arslan, and M. Ali, "High-gain pattern reconfigurable MIMO antenna array for wireless handheld terminals," *IEEE Trans. Antennas Propag.*, vol. 64, no. 10, pp. 4306–4315, Oct. 2016.
[37] *The DARPA ACT Program*. Accessed: Mar. 2014. [Online]. Available: http://www.ofcm.noaa.gov/wg-mpar/meetings/2013-02/07%20ACT.pdf
[38] N. A. Bishop, J. Miller, D. Zeppettella, W. Baron, J. Tuss, and M. Ali, "A broadband high-gain bi-layer LPDA for UHF conformal load-bearing antenna structures (CLASs) applications," *IEEE Trans. Antennas Propag.*, vol. 63, no. 5, pp. 2359–2364, May 2015.
[39] M. D. Wright, "Structurally integrated reconfigurable wideband array for conformal applications," Ph.D. dissertation, Dept. Elect. Eng., Univ. South Carolina, Columbia, SC, USA, Jan. 2018.
[40] *Radant MEMS*. Accessed: Mar. 2014. [Online]. Available: http://www.radantmems.com/radantmems.data/Library/Radant-Datasheet101_1.3.pdf
[41] Wireless Research Center of North Carolina. Accessed: Oct. 2013. [Online]. Available: http://wirelesscenter-nc.org/
[42] D. M. Pozar, *Microwave Engineering*, 4th ed. Hoboken, NJ, USA: Wiley, 2012.

Michael D. Wright (S'13) received the B.Sc. degree in electrical engineering from the University of South Carolina, Columbia, SC, USA, in 2013. In January 2018, he successfully defended his Ph.D. dissertation entitled "Structurally Integrated Reconfigurable Wideband Array for Conformal Applications."

During his research, he was afforded the opportunity to spend a full year as a Research Assistant at the Air-Force Research Laboratory, Wright-Patterson Air Force Base, OH, USA, from 2013 to 2014. He is currently with Ball Aerospace, Boulder, CO, USA. His current research interests include conformal antennas, reconfigurable antennas, structurally integrated antennas, antenna elements for array applications, and extreme wideband and frequency-independent antennas.

William Baron, photograph and biography not available at the time of publication.

Jason Miller, photograph and biography not available at the time of publication.

James Tuss, photograph and biography not available at the time of publication.

David Zeppettella received the B.E. degree in electrical engineering from Youngstown State University, Youngstown, OH, USA, and the M.S. degree in electrical engineering from the University of Dayton, Dayton, OH, USA. He successfully defended his Ph.D. dissertation entitled Multifunction Radio Frequency Composite Structures at the University of South Carolina, Columbia, SC, USA, in 2018.

He is currently an Electronics Engineer with the Aerospace Systems Directorate, Air Force Research Laboratory, Wright-Patterson Air Force Base, OH, USA, where he leads research on multifunction structures. He has 19 years of engineering and research and development experience at laboratories associated with the Department of Defense and the Department of Energy. His current research interests include dual-purpose composite structures for structural state sensing and RF applications.

Mohammod Ali (M'93–SM'03) received the B.Sc. degree in electrical and electronic engineering from the Bangladesh University of Engineering and Technology, Dhaka, Bangladesh, in 1987, and the M.A.Sc. and Ph.D. degrees in electrical engineering from the University of Victoria, Victoria, BC, Canada, in 1994 and 1997, respectively.

From 1998 to 2001, he was with Ericsson Inc., Research Triangle Park, NC, USA. Since 2001, he has been with the Department of Electrical Engineering, University of South Carolina, Columbia, SC, USA, where he is currently a Professor. He had held appointment as a Visiting Research Scientist with the Motorola Corporate EME Research Laboratory, Plantation, FL, USA, in 2004. In 2010 and 2011, he was a Summer Faculty Fellow at the Air Force Research Laboratory (AFRL), Wright Patterson Air Force Base, OH, USA. He also spent a year on sabbatical leave at AFRL from 2013 to 2014. He has authored or co-authored over 180 publications, and he holds nine U.S. patents. His current research interests include conformal antennas, reconfigurable antennas, broadband antennas, mm-wave phased array antennas, metamaterials and metasurfaces, aircraft antennas and their coupling reduction, MIMO antennas, and wireless power transfer and wireless sensors.

Dr. Ali was a recipient of the 2003 National Science Foundation Faculty Career Award. He was also a recipient of the College of Engineering and Computing Young Investigator Award, the Research Progress Award, and the Samuel Litman Distinguished Professor Award from the University of South Carolina in 2006, 2009, and 2011, respectively. He was the Technical Program Co-Chair of the IEEE Antennas and Propagation Society's International Symposium, Charleston, SC, USA, in 2009. He was an Associate Editor of the journal IEEE ANTENNAS AND WIRELESS PROPAGATION LETTERS from 2008 to 2013. He serves in the Technical Program Committee of the IEEE Antennas and Propagation Society's (APS) International Symposium. He has organized special sessions for the IEEE IWAT Conference and the IEEE APS Symposia in the past. He has also served in the Technical Program Committee of the IEEE SmartGrid Conference, the European Association for the Antennas and Propagation Conference, and the Asia Pacific Microwave Conference. Currently, he serves on the editorial boards of the *International Journal of RF and Microwave Computer-Aided Engineering* and the *International Journal of Antennas and Propagation* (Hindawi).